

Article www.acsanm.org

Lanthanide-Doped Upconversion Nanoparticle-Cross-Linked Double-Network Hydrogels with Strong Bulk/Interfacial Toughness and Tunable Full-Color Fluorescence for Bioimaging and Biosensing

Shaowen Xie, Baiping Ren, Guo Gong, Dong Zhang, Yin Chen, Lijian Xu, Changfan Zhang, Jianxiong Xu,* and Jie Zheng*



Cite This: ACS Appl. Nano Mater. 2020, 3, 2774-2786



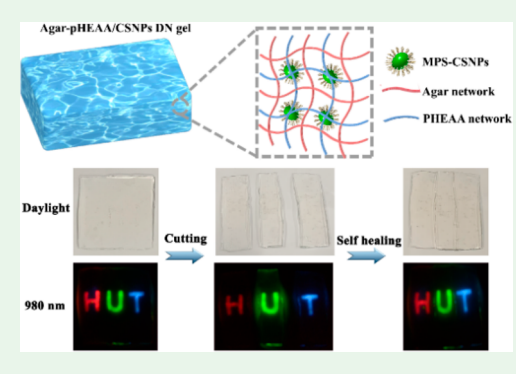
ACCESS

III Metrics & More

Article Recommendations

Supporting Information

ABSTRACT: The design and fabrication of tough and fluorescent hydrogels still remains as a challenging problem due to the poor mechanical property and waterinduced luminescence quenching effect. Here, a new strategy for developing tough and fluorescent hydrogels was proposed by incorporating 3-(trimethoxysilyl)propyl methacrylate (MPS)-functionalized upconversion (UC) fluorescent NaREF₄:Ln³⁺@NaYF₄ core-shell nanoparticles (MPS-CSNPs) into agar/poly(N-(hydroxyethyl)acrylamide) (agar/pHEAA) double-network hydrogels, producing agar/pHEAA@MPS-CSNPs gels. Three typical agar/pHEAA@ MPS-CSNPs gels with RGB-emitting fluorescence were fabricated to exhibit a combination of extraordinary mechanical properties, including high strength (fracture stress of 2.4 MPa), extensibility (fracture strain of 5.6), stiffness (elastic modulus of 1.9 MPa), and toughness (tearing energy of 11000 J/m²), fast self-



recovery (47%/23% toughness/stiffness), excellent self-healing property (self-healing tensile stress/strain of 0.9 MPa/0.9), and superior interfacial toughness of 1100-2000 J/m² on various solid surfaces. In parallel, the full-color UC fluorescence of the hydrogels can be readily tuned from primary RGB colors to any secondary color (even to white color) by simply changing the types and relative ratios of single or multiple MPS-CSNPs. Agar/pHEAA@MPS-CSNPs hydrogels can also retain long fluorescence stability up to 60 days in a dry storage state. Mechanical enhancement and tunable fluorescence in agar/pHEAA@MPS-CSNPs gels are attributed to hybrid cross-linking effects from covalent bonds between abundant vinyl groups on MPS-CSNPs and the second pHEAA network and noncovalent bonds between and within both agar and pHEAA networks. Taking advantage of highly tough, surface adhesion, and self-healing properties, we further fabricated an agar/pHEAA hydrogel film containing fluorescence-responsive patterns for potential anticounterfeiting. We also envision that the agar/pHEAA@MPS-CSNPs hydrogels hold great potential for developing next-generation tough and fluorescent hydrogels for imaging, biosensing, and other optical applications.

KEYWORDS: tough hydrogels, fluorescent hydrogels, upconversion fluorescence, lanthanide-doped nanoparticles, double network

1. INTRODUCTION

Smart fluorescent hydrogels as rising-star optical materials have been broadly explored for different fundamental and practical researches in fluorescent sensors, probes, imaging agents, photocatalysts, and light-emitting devices 1-5 because of their unique color change properties in absorption (chromogenic) or in emission (fluorochromic) in response to external stimulus such as humidity, temperature, pH, light, ionic strength, and mechanical force. A general straightforward approach for preparing fluorescent hydrogels is to incorporate fluorescent materials (e.g., fluorophores and chromophores) into the networks of hydrogels. There are two typical organic and inorganic fluorescent materials with different fluorescence mechanisms. Organic fluorescent materials generally trigger fluorescence emission via unsaturated conjugation and extended π -cloud architectures, while inorganic fluorescent materials are often electronically excited from the ground state

to the higher vibrational and rotational energy states. Fluorescent hydrogels possess unique advantages for achieving from the intrinsic optoelectronic properties of fluorophores/ chromophores and their stimuli-responsive properties of noncovalent interactions (e.g., hydrogen bonding, π -stacking interactions, host-guest interactions, metal coordination, and electrostatic interactions). However, several main obstacles still remain for the design of new fluorescent hydrogels. First, since most of organic fluorescent materials are intrinsically hydrophobic, the incorporation of hydrophobic luminescent

January 13, 2020 Received: Accepted: March 4, 2020 Published: March 4, 2020



materials into highly hydrophilic hydrogels is very difficult. Second, existing fluorescent hydrogels are mechanically weak, and the loss of mechanical strength and stability of fluorescent hydrogels will in turn affect molecular structures or assembled states of fluorophores/chromophores (e.g., spiropyran), leading to luminescence quenching. Third, luminescence is also highly dependent on local environments (e.g., solvent, additives, and polymers), so a high content of water molecules in hydrogels often quenches the luminescence of fluorophores and chromophores. Thus, design and fabrication of fluorescent hydrogels with a combination of tunable luminescence, superior mechanical strength, self-recovery, self-healing, and surface adhesion still remains as a challenging work.

Lanthanide-doped upconversion materials (LnUCMs), such as lanthanide-doped carbon nanotubes,8 lanthanide-organic frameworks, lanthanide-doped alkaline metal tungstates, 10 polymeric lanthanide complexes, 11 and lanthanide-doped fluoride compounds, 12-15 have been reported to possess excellent upconversion luminescent properties due to the abundant energy level pattern of trivalent lanthanide ions stemming from their 4f native intraconfigurational transitions, electronic repulsion, and spin-orbit coupling. LnUCMs often exhibit the typical anti-Stokes emission behavior, which can upconvert the lower energy NIR light to short-wavelength and higher energy emissions via multiphoton cross-relaxation processes, leading to strong luminescence emissions with a broad range of excitation wavelengths spanning from the UV to visible regions and with minimal luminescence quenching effect. 16-20 Among LnUCMs, lanthanide-doped NaREF₄ upconversion nanoparticles (UCNPs) have recently received enormous attention because of their unique photophysical properties (e.g., strong, size-tunable, and multicolor fluorescence, long luminescence lifetime, and high emission stability against photobleaching and photoblinking), nontoxic biocompatibility, environmentally friendly, and ease of surface functionalization. 21-25 A number of studies have reported that UCNPs can be incorporated into poly(*n*-isopropylacrylamide), ^{26,27} poly(methyl methacrylate), ²⁸ polystyrene, ²⁹ poly(vinyl chloride), ³⁰ polyurethane, ³¹ polydimethylsiloxane, ³² and very few hydrogels to realize different stimuli-responsive luminescence functions. 33-36

Several UCNPs-based hydrogels have been developed by incorporating UCNPs into a single polymer network, producing nanocomposite hydrogels (NC gels) with hybrid network structures and fluorescent functions. Zhang et al.³⁷ synthesized a NC hydrogel by cross-linking hemicellulose and ricinoleic acid-coated NaYF4:Yb/Er nanocrystals into hydrogels networks containing poly(N-isopropylacrylamide) and polyacrylamide to achieve both UC luminescence- and temperature-responsive properties. Yan and co-workers³⁵ reported a photosensitive hybrid hydrogel of poly-(acrylamide-ethylene glycol) loaded with NaYF4:Yb/Tm UCNPs for the release of entrapped biomacromolecules. Dong et al.³³ fabricated NaYF₄:Yb,Er nanoparticle-incorporated polyacrylamide hydrogels, but with very weak tensile stress of 20 kPa. However, most of the UCNPs-based hydrogels, not limited to above-mentioned ones, exhibited either weak mechanical properties or poor self-recovery/selfhealing property, not even mentioned to their surface adhesion property. Also, UCNPs-based hydrogels often suffer from the water-induced luminescence quenching effect due to the hydration of lanthanides ions. Beyond UCNPs-based hydrogels, not all tough hydrogels can be anchored onto solid

surfaces, or vice versa, presumably due to different intermolecular interactions between bulk toughness and interfacial toughness. Only a few hydrogels, including agar/pHEAA, poly(2-acrylamido-2-methylpropanesulfonic acid)/polyacrylamide, polyacrylamide/alginate, and Agar/pAAEE (N-poly(acryloylaminoethoxyethanol)), possess high surface adhesive property (bulk toughness of \sim 650–7000 J/m² and interfacial toughness of \sim 650–7000 J/m².)

To simultaneously achieve a combination of superior luminescence and mechanical properties of hydrogels, here we designed, prepared, and characterized a hybrid nanocomposite and double-network hydrogel by using 3-(trimethoxysilyl)propyl methacrylate (MPS)-functionalized NaREF₄:Ln³⁺@NaYF₄ core-shell nanoparticles (MPS-CSNPs) as nano-cross-linkers to copolymerize with agar/ pHEAA double-network (DN) gels. The resultant agar/ pHEAA@MPS-CSNPs gels contain a unique CSNP-crosslinked double-network structure made of a physically linked agar first network and a CSNP-cross-linked pHEAA second chemical network. Thanks to the presence of different functional groups of -OH and -C=C- on the surface of CSNPs, these functional groups allow CSNPs to physically cross-link with the agar network via hydrogen bonds and to chemically cross-link with the pHEAA network via covalent bonds. Such hybrid physically chemically cross-linked networks enable to dissipate energy at different deformation states. Collective data from tensile, tearing, and loading-unloading tests showed the CSNP-enhanced mechanical properties of agar/pHEAA@MPS-CSNPs gels. Specifically, at optimal conditions, agar/pHEAA@MPS-CSNPs bulk hydrogels exhibited superior mechanical strength (fracture stress of 2.4 MPa, fracture strain of 5.6, elastic modulus of 1.9 MPa, and tearing energy of 11000 J/m²), fast self-recovery (toughness/ stiffness recovery of 47%/23% after 30 min resting at elevated temperatures of 95 °C,) and excellent self-healing property (self-healed stress/strain of 0.9 MPa/0.9 at 95 °C for 12 h). Moreover, agar/pHEAA@MPS-CSNPs hydrogels can also readily, directly, and strongly anchored onto different nonporous solid substrates of glass, titanium, aluminum, and ceramics without any surface modification, as demonstrated by high interfacial toughness of 1200-2000 J/m². Apart from superior bulk and interfacial mechanical properties, agar/ pHEAA@MPS-CSNPs hydrogels were able to emit UC colors from primary RGB colors to any secondary color, even to white color by tailoring the types and contents of CSNPs. We hope this work will provide a new structural-based design of mechanical tough and luminescent tunable hydrogels, which are promising for multimodal optical materials and applications.

2. MATERIALS AND METHODS

2.1. Materials. All rare-earth chloride complexes were obtained from Alfa Aesar. Agar (gel strength >300 g·cm⁻²), initiator Irgacure 2959, oleic acid (90%), 1-octadecence (90%), 3-(trimethoxysilyl)-propyl methacrylate (98%), tetraethyl orthosilicate (98%), IGEPAL-CO-520, and NaOH (99%) were purchased from Sigma-Aldrich. *N*-(Hydroxyethyl)acrylamide (>98%) and sodium oleate (>97.0%) was obtained from TCI America. Ammonium fluoride (NH₄F, 99%) was obtained from Acros. The Ln(oleate)₃ complexes were synthesized as reported in our previous work by the reaction of rare-earth chloride and sodium oleate. All materials were used directly without purification. Deionized water employed in our work was purified by a Millipore water purification system.

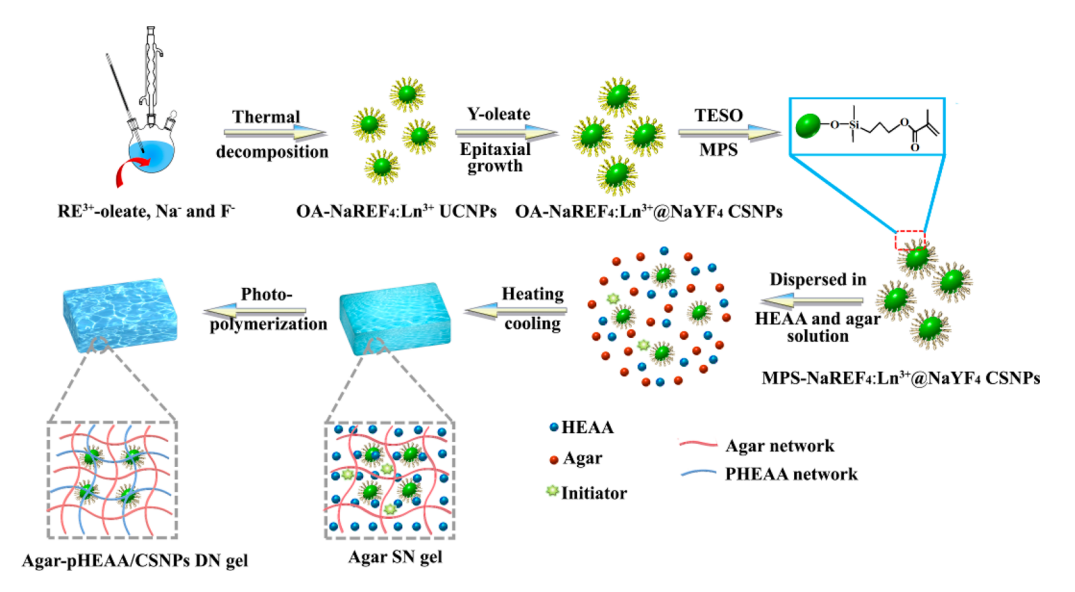


Figure 1. Scheme of the stepwise preparation of agar/pHEAA@MPS-CSNPs hydrogels.

2.2. Synthesis of NaREF₄:Ln³⁺@NaYF₄ CSNPs (RE = Y and Er, Ln³⁺ = Yb/Er, Yb/Tm, and Tm). The synthesis of NaREF₄:Ln³⁺@NaYF₄ CSNPs was achieved by sequential two steps including preparation of NaREF₄:Ln³⁺ UCNPs by a simple thermal decomposition method by using Ln(oleate)₃ complexes as precursors⁴³ and epitaxial growth of an inert NaYF₄ shell on the surface of UCNPs via an oleic acid-mediated thermal decomposition process. The experimental details can be found in our recent works.¹⁹

2.3. Surface Modification of CSNPs. The surface modification of CSNPs was synthesized by adopting an inverse microemulsion procedure. Typically, the above 1 mL cyclohexane solution containing 30 mg of CSNPs and 1 g of CO-520 was dispersed in 10 mL of cyclohexane and stirred for 30 min. Afterward, 0.15 mL of NH₄OH was added into the reaction solution and then stirred for 30 min. Then, 0.08 mL of TEOS was added into the solution and stirred for 24 h under ambient temperature. Subsequently, 0.02 mL of MPS was added in the reaction system and stirred for 24 h. Finally, 20 mL of acetone was added into the reaction solution to precipitate the products (denoted as MPS-CSNPs) and washed several times with acetone. Finally, the MPS-CSNPs sample was obtained as a solid form by lyophilization.

2.4. Synthesis of Agar/pHEAA@MPS-CSNPs Gels. The agar/ pHEAA@MPS-CSNPs gel was synthesized by using a similar method as our reported previously. 45 Briefly, 3.6 g of N-(hydroxyethyl)acrylamide (HEAA), 0.36 g of agar, 0.0612 g of initiator Irgacure 2959 (1 mol % of HEAA), 3 mL of water, and a certain amount of MPS-CSNPs were added into a reactor under N2 protection after degassing several times. Then, the reactor transformed to a preheated water bath of 95 °C for about 10 min to dissolve all the reactants and form agar/ pHEAA@MPS-CSNPs sols. Afterward, the agar/pHEAA@MPS-CSNPs sols was injected into a glass mold containing 1 mm thick Teflon spacer. After being cooled naturally, the physically linked agar first network was formed. Then, glass mold contained agar network, and other unreacted reactants were photopolymerized by UV light for 1 h to form agar/pHEAA@MPS-CSNPs gels. The contents of MPS-CSNPs in the gels were 0.1-1.0 wt % of total reactants. All agar/ pHEAA@MPS-CSNPs gels were prepared in the same way just by tailoring the types and contents of CSNPs in the gels. To further distinguish different agar/pHEAA@MPS-CSNPs gels, the resultant agar/pHEAA@MPS-CSNPs gels were named CSNPs-Xy gels, where X and Y denote the types and contents of MPS-CSNPs in the gels, respectively. For example, the CSNPs-G_{0.2} gels were prepared by adding 0.2 wt % MPS-CSNPs-G in the above method.

2.5. Fabrication of Self-Healing Hydrogel Film with Anticounterfeiting Pattern. The self-healing hydrogel film with anticounterfeiting pattern was fabricated by first molding with agar/

pHEAA@MPS-CSNPs gels to form luminescent anticounterfeiting pattern and then casting into film with the agar/pHEAA gels. First, agar/pHEAA@MPS-CSNPs sols with RGB luminescence were injected into a Teflon mold with "HUT" patterns. To maintain the three letters with similar perceived upconversion brightness, the letter "H" was filled with CSNPs-R $_{0.5}$ sols, "U" was filled with CSNPs-G $_{0.2}$ sols, and "T" was filled with CSNPs-B $_{0.3}$ sols. The agar/pHEAA@MPS-CSNPs sols in molds were gradually cooled naturally to form an agar gels network and photopolymerized for 1 h under UV light to form solidified "HUT" gel patterns. Then, the "HUT" patterns were further put into a Teflon mold (5 \times 5 cm²), followed by injection of hot agar/pHEAA sols into the Teflon mold, cooldown, and photopolymerization under UV light to form an agar/pHEAA self-healing hydrogel film with the "HUT" luminescent pattern.

2.6. Physical Characterization. A JEOL JEM-1230 transmission electron microscope (TEM) operating at 120 kV was adopted to analyze the morphology and size of nanoparticles. A Thermo Scientific Nicolet 6700 spectrometer were used to perform Fourier transform infrared spectroscopy (FTIR) experiments. All upconversion luminescence spectra were measured on a PerkinElmer LS55 spectrometer coupled with an external 980 nm NIR laser (5 W). The fluorescent photographs were visualized under the excitation of 980 nm diode laser and recorded on a cell phone. The used of spot area for laser beam was fixed at 0.125 mm².

2.7. Mechanical Tests. Tension Tests. Uniaxial tensile tests of asprepared gels sample with 25 mm in gauge length, 3.18 mm in width, and 1 mm in thickness were performed on a tensile tester equipped with a 100 N load cell. The stretching speed was fixed at 100 mm/min. For hysteresis measurement, the as-prepared gels sample were stretched to a preset extension ratio and then unloaded. And for recovery experiments, the gels sample was coated with paraffin stored at 95 °C after a second loading—unloading test to avoid water volatilization. After the sample gel was cooled to normal temperature, the next loading—unloading test was conducted. For successive loading—unloading tests, the same gels sample was stretched to an increasing strain until it broke.

Tearing Test. Tearing tests of rouser-shaped sample gels (a length of 40 mm, a width of 20 mm, and a thickness of 1 mm) with an initial notch of 20 mm were performed using the above tensile tester. Before the test, two arms of the gels sample were clamped, while the other arm was stretched upward at 100 mm/min. The tearing energy is estimated by $T = 2F_{\rm max}/\omega$, where $F_{\rm max}$ is the force of peak values of testing curve and ω is width of the specimen.

Self-Healing Tests. The gels sample (thickness of 1 mm) was cut into two specimens, and then the fresh cutting surfaces of two specimens were put together. Subsequently, these two specimens was

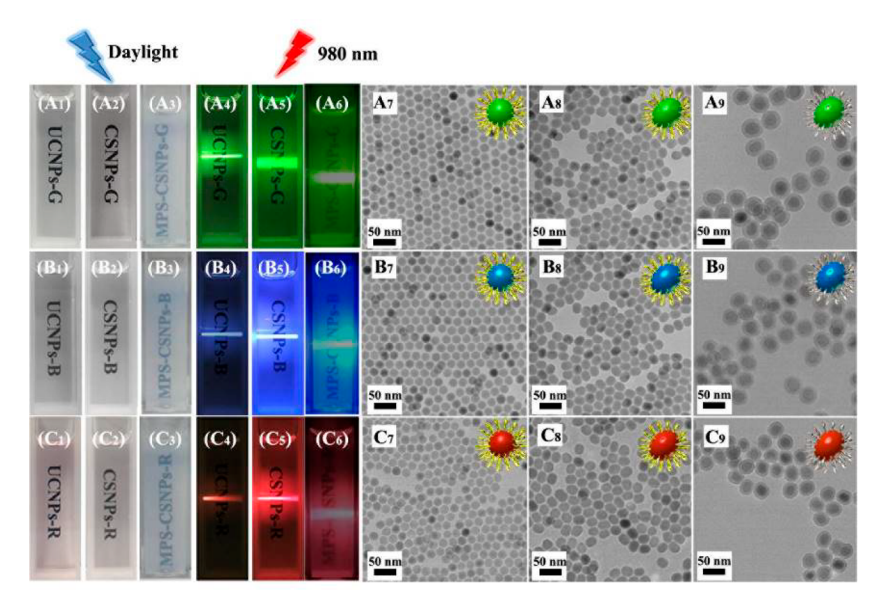


Figure 2. Morphological and optical properties of different types of UCNPs, CSNPs, and MPS-CSNPs, including (A) UCNPs-G, CSNPs-G, and MPS-CSNPs-G, (B) UCNPs-B, CSNPs-B, and MPS-CSNPs-B, and (C) UCNPs-R, CSNPs-R, and MPS-CSNPs-R. Under daylight, no obvious color emission was observed for (A_1-A_2) UCNPs-G and CSNPs-G, (B_1-B_2) UCNPs-B and CSNPs-B, (C_1-C_2) UCNPs-R and CSNPs-R in cyclohexane solution as well as (A_3) MPS-CSNPs-G, (B_3) MPS-CSNPs-G, and (C_3) MPS-CSNPs-G in aqueous solution. Under a 980 nm laser, (A_4-A_6) UCNPs-G, CSNPs-G, and MPS-CSNPs-B, CSNPs-B, and MPS-CSNPs-B, (C_4-C_6) UCNPs-R, CSNPs-R, and MPS-CSNPs-R emit UC green, blue, and red luminescence to different extents, respectively. TEM images of (A_7) UCNPs-G, (A_8) CSNPs-G, (A_9) MPS-CSNPs-G, (B_7) UCNPs-B, (B_8) CSNPs-B, (B_9) MPS-CSNPs-B, (C_7) UCNPs-R, (C_8) CSNPs-R, and (C_9) MPS-CSNPs-R to show their uniform structural morphologies and size distributions. The corresponding molecular structures, as shown in the inset images in (A_7-A_9) , (A_7-A_9) , (A_7-C_9) , are determined by molecular modeling.

placed into the mold and sealed at room temperature or elevated temperature (95 °C) for 12 h. After healing, the mechanical property of healed gels was performed by using the above tensile tests.

Peeling Tests. The gel sample was prepared in a mold with a solid substrate (titanium, ceramic, aluminum, and glass) and a Teflon spacer (16 mm × 65 mm × 3 mm). The 90° peeling tests with a 90° fixture were conducted to analyze the interfacial toughness between the gels and the solid substrates. Before the test, the upside of gels was anchored onto the Scotch duct tape (3M) as a stiff backing for the peeling test. Finally, the gels sample was analyzed with the 90° peeling tests by using a universal tensile tester at a fixed crosshead speed of 50 mm/min. The interfacial toughness (g) were estimated by $g = F_{\text{max}}/\omega$, where F_{max} is the maximum force of the testing curve and ω is the width of the gel sample.

3. RESULTS AND DISCUSSION

Figure 1 shows the general synthesis of agar/pHEAA@MPS-CSNPs gels by using MPS-CSNPs as nano-cross-linkers and fluorophores to copolymerize with agar/pHEAA DN gels. To this end, we first synthesized NaREF₄:Ln³⁺ UCNPs using the thermal decomposition strategy. To promote the UC emission efficiency of NaREF4:Ln3+ UCNPs, an inert NaYF4 shell was grown epitaxially on the surface of NaREF4:Ln3+ UCNPs. In this way, the inert NaYF4 shell could greatly decrease the nonradiative decay of a NaREF4:Ln3+ core of UCNPs caused by surface defects and vibrational deactivation from solvent molecules and ligands. Moreover, to render the as-obtained NaREF₄:Ln³⁺@NaYF₄ CSNPs water dispersible and to introduce the double-bond-terminated groups for the further gelation process, the surface of NaREF₄:Ln³⁺@NaYF₄ CSNPs was further modified by a uniform silica layer through hydrolyzing tetraethoxysilane (TESO) and coupling agent [3-(methacryloyloxy)propyl]trimethoxysilane (MPS) in a reverse microemulsion system, thus ultimately producing hydrophilic MPS-CSNPs with pendent double bonds. Upon

obtaining MPS-CSNPs, they were redispersed into an aqueous solution containing agar, HEAA, and UV initiator. After that, the mixture solution was heated to 95 °C for 10 min and then gradually cooled to form a physically linked agar first network in the presence of HEAA monomers, MPS-CSNPs, and UV initiator via the thermo-induced sol—gel transition. Finally, the pHEAA@MPS-CSNPs second chemical network was prepared by introducing the UV light to photopolymerize HEAA monomers.

3.1. Morphological and Fluorescent Properties of UCNPs, CSNPs, and MPS-CSNPs. As a proof-of-concept, three typical types of lanthanide-doped NaYF4:Yb,Er UCNPs (UCNPs-G), NaErF4:Tm UCNPs (UCNPs-R), and NaY-F₄:Yb,Tm UCNPs (UCNPs-B) that emit green, red, and blue color, respectively, were first prepared by using the two-step thermal decomposition method as described above. 18,46,47 As shown in Figures 2A7, 2B7, and 2C7, all three types of UCNPs-G, UCNPs-B, and UCNPs-R exhibited very uniform spherical shape and size distribution. The average size of three types of UCNPs was about ~24 nm. Next, to minimize the nonradiative decay and the enhance UC emission efficiency of UCNPs, an optically inert NaYF4 shell layer was coated on the surface of three types of NaREF₄:Ln³⁺ UCNPs to produce NaYF₄:Yb,Er@NaYF₄ CSNPs (CSNPs-G), NaYF₄:Yb,Tm@ NaYF₄ CSNPs (CSNPs-B), and NaErF₄:Tm@NaYF₄ CSNPs (CSNPs-R). Figures 2A₈-C₈ show that upon coating of an inert layer three NaREF4:Ln3+@NaYF4 CSNPs had uniform elliptical shapes. The length of the elliptical-shape CSNPs was \sim 36 nm, while the width was \sim 32 nm. Next, a silica layer with pendent double bonds was coated on NaREF₄:Ln³⁺@NaYF₄ CSNPs to produce MPS-NaYF₄:Yb,Er@NaYF₄ CSNPs (MPS-CSNPs-G), MPS-NaYF₄:Yb,Tm@NaYF₄ CSNPs (MPS-CSNPs-B), and MPS-NaErF₄:Tm@NaYF₄ CSNPs (MPS-

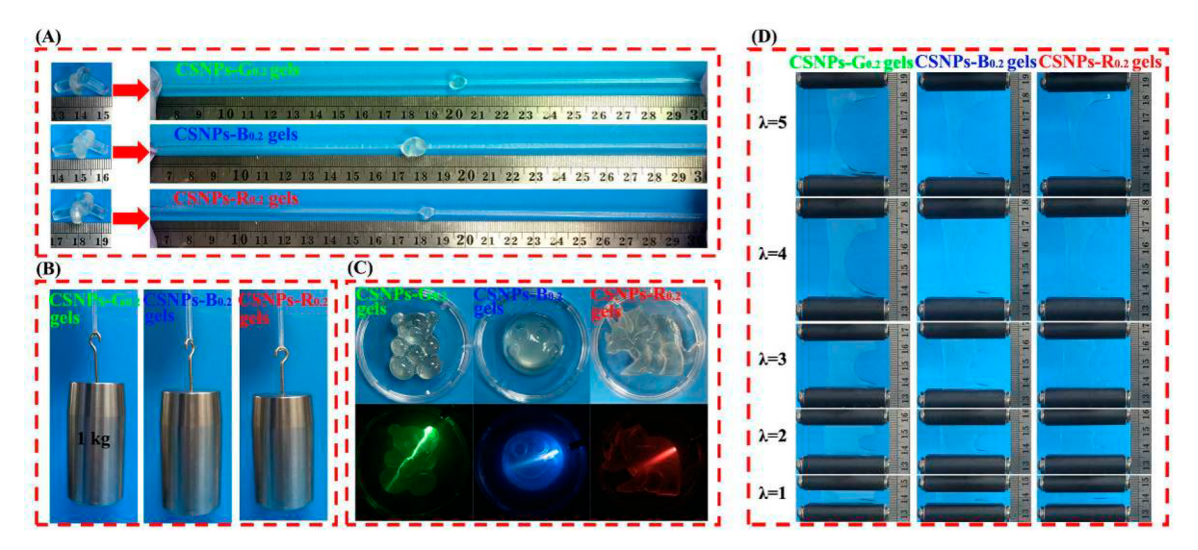


Figure 3. Visual photograph of mechanical and fluorescence properties of three agar/pHEAA@MPS-CSNPs gels, as evidenced by (A) knotted stretching, (B) holding 1 kg of weight, (C) forming different complex shapes with very fine structures of a bear, smiling face, and dinosaur, which emit distinct green, blue, and red UC fluorescence under a 980 nm laser irradiation, and (D) resisting crack propagation.

CSNPs-R), with the increased size of ~45 nm due to the formation of the SiO2 with the thickness of ~10 nm and almost unchanged shape and size monodispersity (Figures 2A₉-C₉). Quantitatively, FTIR was used to examine whether the surfaces of three CSNPs were successfully modified by the silica layer. As shown in Figure S1A, before surface modification by TEOS and MPS, all three CSNPs exhibited typical peaks of OA molecules at 3434, 2932, 2864, 1569, and 1467 cm⁻¹. Among them, the bands around 3434 cm⁻¹ were associated with the stretching vibration of the hydroxyl group. The asymmetric and symmetric stretching vibrations of the carboxylic group (COO⁻) can be proved by two peaks at 1569 and 1467 cm⁻¹. Furthermore, two peaks at 2932 and 2864 cm⁻¹ corresponded to the asymmetric and symmetric stretching vibrations of methylene group. All these peaks were confirmed presence of oleic acid molecule on the surface of CSNPs.⁴⁸ After coating of a silica layer, some new Siassociated peaks were observed in Figure S1B, including the amorphous silica Si-O-Si vibration at 1093 and 794 cm⁻¹, the Si-OH vibration at 950 cm⁻¹, free Si-OH groups at 3749 cm⁻¹, and hydrogen-bonded Si-water at 3420 cm⁻¹.49 Furthermore, two new bands at 1722 and 1635 cm⁻¹ were observed and assigned to the stretching vibration of double carbon bond (C=C) and carbanyl group (C=O) of MPS, respectively. Clearly, the presence of all these new peaks confirms that silica layers with pendent double bonds were successfully coated on the surface of three CSNPs. 44,5

With regard to optical properties, hydrophobic NaR-EF₄:Ln³⁺ UCNPs and NaREF₄:Ln³⁺@NaYF₄ CSNPs with OA-functionalized surfaces exhibited no optical emission in a cyclohexane solution under daylight (Figures $2A_1$ – A_2 , B_1 – B_2 , C_1 – C_2). However, after silica-shell surface modification of NaREF₄:Ln³⁺@NaYF₄ CSNPs, the resultant MPS-NaR-EF₄:Ln³⁺@NaYF₄ CSNPs became highly hydrophilic. Hence, the as-obtained MPS-NaREF₄:Ln³⁺@NaYF₄ CSNPs can be well dispersed in aqueous solution and form a homogeneous colloidal solution (Figures $2A_3$, B_3 , C_3). Upon excitation by the 980 nm laser, NaREF₄:Ln³⁺ UCNPs, NaREF₄:Ln³⁺@NaYF₄ CSNPs emitted distinct green (A_4 – A_6), blue (B_4 – B_6), and red (C_4 – C_6) luminescence, respectively. Moreover, the fluorescent spectra

in Figure S2A show that UCNPs-G, CSNPs-G, and MPS-CSNPs-G exhibited typical upconversion fluorescent emission peaks at the same positions of 409, 527, 541, and 655 nm, corresponding to the transitions of ${}^2H_{9/2}-{}^4I_{15/2}$, ${}^2H_{11/2}-{}^4I_{15/2}$, ${}^4S_{3/2}-{}^4I_{15/2}$, and ${}^4F_{9/2}-{}^4I_{15/2}$ of Er^{3+} , respectively. Clearly, the green emission peaks at 527 and 541 nm were significantly higher than the other peaks. Consistently, visual inspection showed green UC emission under the irradiation of a 980 nm laser (inset in Figure S2A). After the epitaxial growth of the NaYF₄ shell, CSNPs-G emitted 8 times higher UC luminescence than UCNPs-G, confirming that the presence of the NaYF₄ shell can indeed suppress the surface-induced quenching effect of a NaREF₄:Ln³⁺ core of UCNPs. However, the photoluminescence of MPS-CSNPs-G decreased to some extent as compared to that of CSNPs-G due to the surface hydration-induced quenching effect.⁵¹

In the cases of UCNPs-B, CSNPs-B, and MPS-CSNPs-B, two strong blue-color emission peaks at 450 and 475 nm were observed. Meanwhile, a very weak peak at 644 nm was detected (Figure S2B). These three peaks were assigned to the $^{1}D_{2}-^{3}F_{4}$, $^{1}G_{4}-^{3}H_{6}$, and $^{1}G_{4}-^{3}F_{4}$ transitions of Tm³⁺, respectively. Obviously, the intensity of blue-emission peaks located at 450 and 475 nm were significantly higher than that of the red-emission peak; these three types of nanoparticles still exhibited a dominant blue-emission color under the irradiation of a 980 nm laser (inset in Figure S2B). Similarly, UC florescence enhancement of UCNPs-B was observed after coating the NaYF₄ shell. For red-emitted nanoparticles, the red emission of CSNPs-R at 654 nm via a ${}^4F_{9/2} - {}^4I_{15/2}$ transition was significantly enhanced after coating a NaYF4 shell on the UCNPs-R (Figure S2C). This is attributed to the luminescence quenching in the UCNPs-R, as mainly induced by rapid energy migration, not cross-relaxation.⁵² Furthermore, after coating a NaYF4 shell, the luminescence quenching effect in CSNPs-R was largely suppressed, endowing the CSNPs-R with bright red emission (inset in Figure S2C).

3.2. Mechanical Properties of Agar/pHEAA@MPS-CSNPs Hydrogels. Upon synthesis of MPS-CSNPs with tunable UC fluorescence, good water-dispersion ability, and double-bond-terminated functional groups, we then used three MPS-CSNPs as nano-cross-linkers and fluorophores to

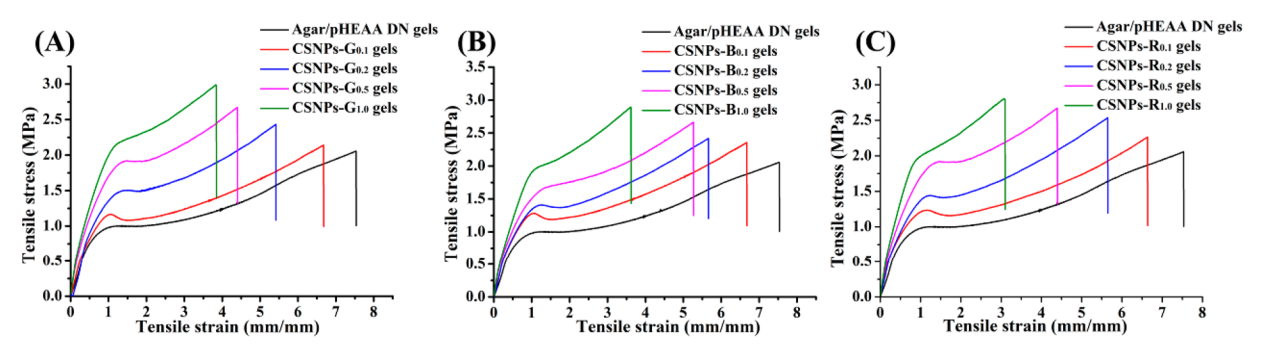


Figure 4. Concentration effect of MPS-CSNPs on tensile properties of (A) CSNPs-G gels, (B) CSNPs-B gels, and (C) CSNPs-R gels.

copolymerize with physically cross-linked agar/pHEAA, forming fluorescent agar/pHEAA@MPS-CSNPs gels with pure green, blue, and red upconversion emission. At a first glance in Figure 3, three agar/pHEAA@MPS-CSNPs gels (CSNPs-G_{0.2} gels, CSNPs-B_{0.2} gels, and CSNPs-R_{0.2} gels) displayed excellent mechanical properties. All three agar/ pHEAA@MPS-CSNPs gels can be knotted and stretched to about 10 times its original length (Figure 3A). These three gels can also hold a weight of 1 kg without breakage (Figure 3B). Moreover, the as-prepared agar/pHEAA@MPS-CSNPs gels are flexible and can adapt various complex shapes with fine structures, including a bear, smiling face, and dinosaur (Figure 3C), indicating their free-shapeable properties. Meanwhile, these gels exhibited distinct green, blue, and red UC fluorescence under 980 nm laser irradiation. Figure 3D shows the crack propagation process of the three notched agar/pHEAA@MPS-CSNPs gels. Obviously, the initial crack blunting tip can be turned gradually into a semicircular-shaped crack as a tensile strain (λ) increased from 0 to 5, demonstrating excellent toughness of the three agar/ pHEAA@MPS-CSNPs gels. All these qualitative results showed that the as-prepared agar/pHEAA@MPS-CSNPs gels possess both high mechanical and tunable UC fluorescence.

To quantitatively study the MPS-CSNPs-induced reinforcement mechanism of agar/pHEAA@MPS-CSNPs gels, a series of tensile tests were performed to analyze the effects of MPS-CSNPs contents on mechanical properties of three agar/ pHEAA@MPS-CSNPs. The contents effects of agar and pHEAA components on mechanical properties of agar/ pHEAA DN gels have already been studied in our previous works.³⁸ Figure 4 illustrates the tensile stress-strain curves of the three MPS-CSNPs-cross-linked hydrogels with different MPS-CSNPs contents. Clearly, pure physical agar/pHEAA DN gels without MPS-CSNPs showed a fracture stress of ~2.0 MPa at a fracture strain of 7.6. Upon introducing different fluorescent MPS-CSNPs, agar/pHEAA@MPS-CSNPs gels exhibited different mechanical properties from pure agar/ pHEAA DN gels. For example, CSNPs-G gels can be increased their tensile stress from 2.3 to 2.9 MPa but decrease their fracture strains from 6.7 to 3.6 as MPS-CSNPs-G concentrations increased from 0.1 to 1.0 wt %. Similarly, CSNPs-B gels and CSNPs-R gels showed the enhanced tensile stress at the expense of tensile strains (Figures 4B,C). These results indicate that the increase of cross-linker density of MPS-CSNPs, on the one hand, enhances network association and tensile stress and shortens effective chain lengths in the networks, on the other hand. Therefore, the chain dynamics of gels were restricted and fractured at low strains.

In parallel to tensile properties, we also examined the tearing energy of three MPS-CSNPs-cross-linked hydrogels as a function of MPS-CSNPs contents. Figure S3A shows a typical tearing energy curve of CSNPs-G gel with 0.2% MPS-CSNPs (namely CSNPs-G_{0.2} gels). The tearing energy of CSNPs-G_{0.2} was 13459 I/m² as compared to that of pure agar/pHEAA DN gels (8368 J/m²) and articular cartilage (1000 J/m²). Specifically, after cross-linking with MPS-CSNPs-G, the tearing energy of CSNPs-G gels significantly and monotonically increased from 11453 to 18704 J/m² as MPS-CSNPs-G contents increased from 0.1 to 1.0 wt % (Figure S3B). Similarly, CSNPs-B and CSNPs-R gels increased their respective tearing energy from 10296 to 188843 J/m² and from 11605 to 19177 J/m² as the contents of MPS-CSNPs (Figures S3C,D). All the three agar/pHEAA@MPS-CSNPs gels showed remarkably high tearing energy of 10000-18000 I/m², indicating that the introduction of MPS-CSNPs to crosslink the second pHEAA network can indeed play the role as additional sacrificial bonds to dissipate energy efficiently, so endowing the agar/pHEAA@MPS-CSNPs gels with high tearing and tensile properties.

For comparison, we also conducted tensile tests for pHEAA single-network gel (SN gel) and pHEAA@MPS-CSNPs SN gel to determine whether MPS-CSNPs could copolymerize with the second pHEAA network as nano-cross-linkers. As shown in Figure S4, pure pHEAA SN gel without MPS-CSNPs showed a fracture stress of about 0.4 MPa and a fracture strain of ~6.8, while pHEAA@MPS-CSNPs SN gel increased its tensile stress to 0.89 MPa at a fracture strain of about 9.0. These results suggest that MPS-CSNPs indeed cross-link with the pHEAA network to enhance the mechanical properties of pHEAA@MPS-CSNPs SN gel.

3.3. Energy Dissipation of Agar/pHEAA@MPS-CSNPs Gels. Different cyclic loading-unloading tests were conducted to analyze the effects of MPS-CSNPs cross-linking on energy dissipation of three agar/pHEAA@MPS-CSNPs gels and pure agar/pHEAA DN gels.Figures S5A-D show the cyclic loading-unloading curves of pure agar/pHEAA, CSNPs-G_{0.2}, CSNPs-B_{0,2}, and CSNPs-R_{0,2} hydrogels at different strains. All agar/pHEAA@MPS-CSNPs gels displayed distinct hysteresis loops at different strains. In addition, all hysteresis loops of three agar/pHEAA@MPS-CSNPs gels were gradually increased as strain (λ). Quantitatively, as shown in Figure S5E, at lower strains of $\lambda = 1-2$, dissipated energies of pure agar/ pHEAA DN gels were $\sim 0.54 \text{ MJ/m}^3$ at strains of $\lambda = 1$, while the energies increased to $\sim 1.48 \text{ MJ/m}^3$ at strains of $\lambda = 2$, comparable to those of three agar/pHEAA@MPS-CSNPs gels (\sim 0.69 MJ/m³ at strains of $\lambda = 1$ and \sim 1.88 MJ/m³ at strains of $\lambda = 2$). However, at higher strains of $\lambda = 3-5$, the difference

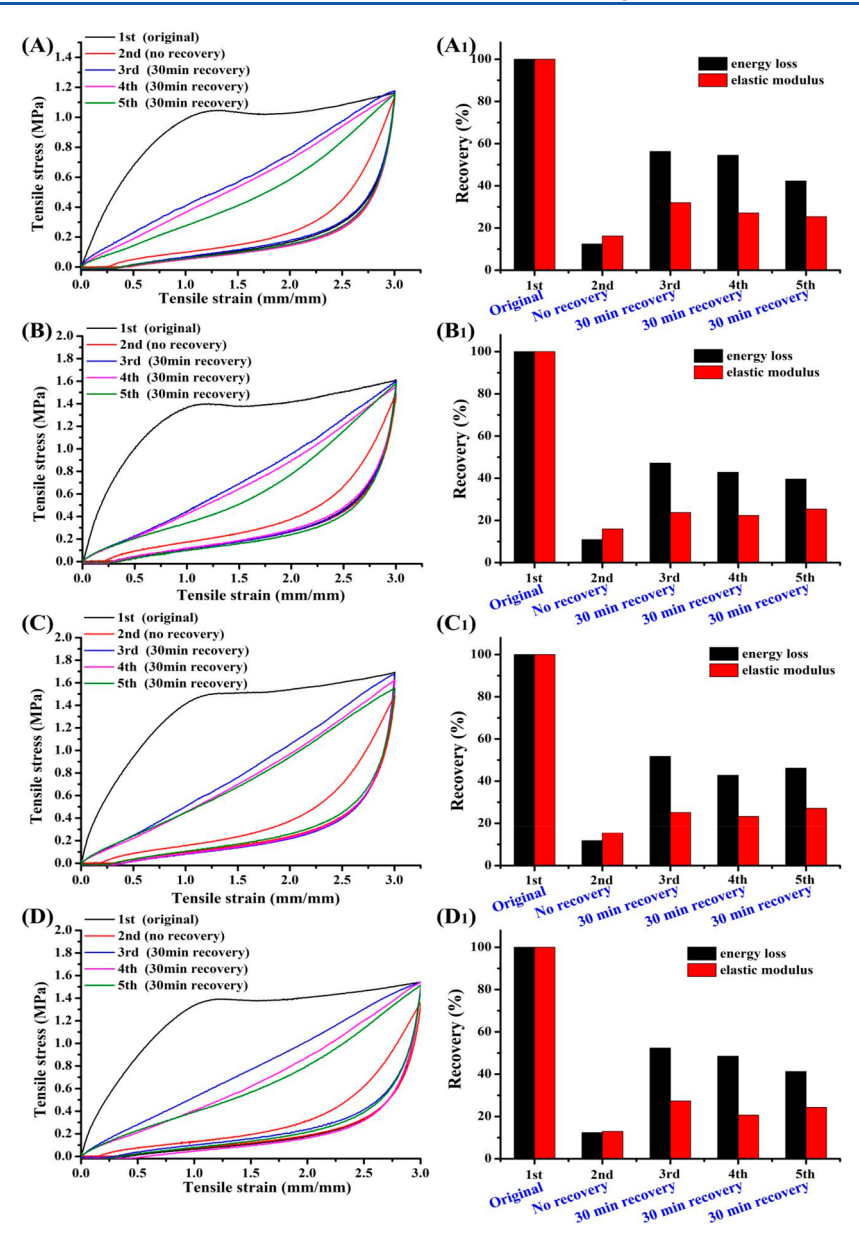


Figure 5. Self-recovery of (A) agar/pHEAA, (B) CSNPs- $G_{0.2}$, (C) CSNPs- $B_{0.2}$, and (D) CSNPs- $R_{0.2}$ gels by five successive loading—unloading tests with a maximum strain of $\lambda = 3$ and 95 °C, with no resting time was given between the original and the second cycle, while 30 min resting was conducted for the third to fifth cycles. (A_1 – D_1) Energy loss and elastic modulus recovery of the four above-mentioned hydrogels, estimated from the stress–strain curves from (A–D).

in dissipated energies between pure agar/pHEAA DN gels and three agar/pHEAA@MPS-CSNPs gels became more obvious. Agar/pHEAA DN gels dissipated energy from $\sim\!2.28$ MJ/m³ at strains of $\lambda=3$ to $\sim\!4.22$ MJ/m³ as the strains increased to $\lambda=5$, while three agar/pHEAA@MPS-CSNPs gels dissipated energy from 3.10 MJ/m³ at strains of $\lambda=3$ to $\sim\!5.80$ MJ/m³ as the strains increased to $\lambda=5$. This indicates that energy-dissipation mode of all three agar/pHEAA@MPS-CSNPs gels changes as strains. At low strains, agar/pHEAA@MPS-CSNPs gels mainly dissipate energy via the fracture of the physically linked agar first network. When the hydrogel subject to the larger strains, both network work together to dissipate energy more efficiently so as to endure high deformation.

In addition, a successive loading—unloading test of the same hydrogels was performed to study the internal energy dissipation process of agar/pHEAA DN gels and three agar/pHEAA@MPS-CSNPs gels at different strains in Figure S6. It

is worth reminding that no resting time was given between any two consecutive loading cycle during a successive loadingunloading test. For the four types of hydrogels tested, they exhibited similar fracture behaviors, i.e., hysteresis loops and tensile stress of all gels increased as strains (Figures S6A-D). On one hand, softening behavior of the gel appears below their yield point and spread continuously with increasing tensile strains. On the other hand, every reloading curve partially overlapped with its previous unloading curve, suggesting that the networks only partially recover from its immediate unloading process. As λ increased from 1 to 5, the tensile stress of agar/pHEAA DN gel increased from 1.07 to 1.26 MPa, while the tensile stresses of three agar/pHEAA@MPS-CSNPs gels increased from 1.40 to 2.10 MPa. In Figure S6E, the energy dissipation of agar/pHEAA DN gels increased from 0.54 to 1.02 MJ/m³ as increasing the tensile stain increased from 1 to 2, but further increase of tensile stain almost did not induce significant change for energy dissipation. Differently, the three agar/pHEAA@MPS-CSNPs gels continuously dissipated more energy as increasing the tensile stain from 1 to 5. For example, the energy dissipation of CSNPs- $G_{0.2}$ gels increased rapidly from 0.69 to 1.33 MJ/m³ as increasing the tensile stain from 1 to 2 and further increased to 1.87 MJ/m³ when the tensile stain was $\lambda = 5$. These results again confirm that MPS-CSNPs can successfully copolymerize with the second pHEAA network to improve mechanical properties.

3.4. Self-Recovery and Self-Healing Properties of Agar/pHEAA@MPS-CSNPs Gels. To gain insight into the effects of reversible nature of hydrogen bonds of both agar and pHEAA networks on the self-recovery property of agar/ pHEAA DN gels and three agar/pHEAA@MPS-CSNPs gels, a series of five loading-unloading cycles with a maximum strain of $\lambda = 3$ were performed at the elevated temperature of 95 °C. For a better comparison, we designed the cyclic loadingunloading tests in a way that no any resting was applied between the first and second cycles, while 30 min resting was conducted for the third, fourth, and fifth cycles. As a control, Figures 5A-A₁ exhibited that the toughness/stiffness recovery ratio of agar/pHEAA DN gels was 56%/32% as evidenced by the larger hysteresis loop of the third recovery cycle, while their toughness/stiffness recovery ratio was only 12%/16% after the second recovery. Without any resting, the fractured networks of agar/pHEAA DN gels cannot be recovered immediately. Furthermore, the toughness/stiffness recovery ratio of agar/ pHEAA DN gels retained at 54%/27% and 45/25% after the fourth and fifth recovery. The results indicated that the mechanical recovery of agar/pHEAA DN gels had the repeatability multiple times at the elevated temperature of 95 °C. Similarly, mechanical recovery was also observed for three agar/pHEAA@MPS-CSNPs gels (Figures 5B-B₁, C-C₁, D-D₁). Specifically, the toughness/stiffness recovery was as low as 10%/15% for CSNPs-G_{0.2}, 11%/16% for CSNPs-B_{0.2}, and 11%/13% for CSNPs-R_{0.2} at the second cycles without any resting. After 30 min resting, three agar/pHEAA@MPS-CSNPs gels allowed to increase and retain toughness/stiffness recovery to 47%/23%, 48%/22%, and 40%/25.4% for CSNPs- $G_{0.2}$ gels, 51%/25%, 42%/23%, and 46%/27% for CSNPs- $B_{0.2}$ gels, and 52%/26%, 48%/20%, and 41%/25% for CSNPs-R_{0.2} gels during the third, fourth, and fifth cycles. Clearly, the three agar/pHEAA@MPS-CSNPs gels had slightly less self-recovery efficacy than agar/pHEAA DN gels, presumably because of the nonrecoverable chemical bonding between pHEAA and MPS-CSNPs.

We further investigated the self-healing property of three agar/pHEAA@MPS-CSNPs gels. As shown in Figure 6A, CSNPs-G_{0.2} and CSNPs-B_{0.2} gels were first cut into four separate gels, and then the two separate gels from different agar/pHEAA@MPS-CSNPs gels were physically anchored together at room temperature for 12 h. After healing, the self-healed gels could be bent to 60°. In addition, the gels of round shape that were healed at 95 °C or 12 h were mechanically strong to withstand stretching by a tweezers (Figure 6B). Both healed gels can also retain their original UC fluorescence. Visual inspection confirmed that three agar/ pHEAA@MPS-CSNPs gels exhibited self-healing and fluorescence properties. Furthermore, the healed gels were subject to tensile tests to quantitatively determine their mechanical properties after healing at room temperature and 95 °C. As shown Figures 6C-F, the healed agar/pHEAA and three agar/ pHEAA@MPS-CSNPs gels at room temperature can be

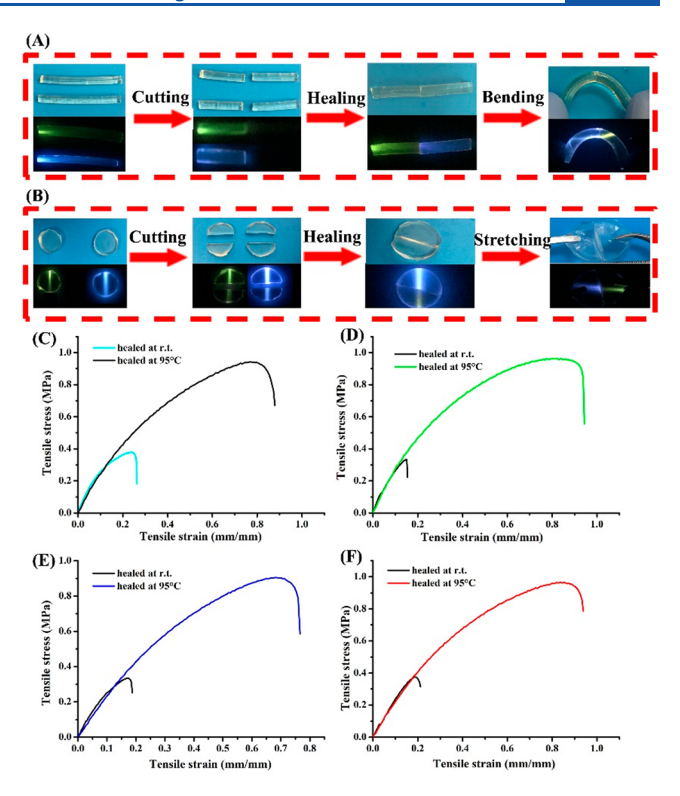


Figure 6. Visual inspection of self-healing performance of agar/pHEAA@MPS-CSNPs gels at (A) room temperature and (B) 95 °C. The self-healed gels not only withstand the bending and stretching but also emit UC fluorescence under the 980 nm excitation. Mechanical tensile tests on the self-healed (C) agar/pHEAA, (D) CSNPs- $G_{0.2}$, (E) CSNPs- $B_{0.2}$, and (F) CSNPs- $R_{0.2}$ gels at 95 °C.

achieved a fracture stress of \sim 0.3 MPa at a strain of 0.2. But, upon healing the hydrogels at the elevated temperature of 95 °C, the four healed gels significantly improved their mechanical properties, as evidenced by 0.9 MPa of tensile stress at fracture strain of 0.9. These results indicate that without the heating process self-healing of four types of hydrogels mainly stems from the re-formation of hydrogel bonds from the second pHEAA network. With heating treatment, the healing effect is largely improved via the sol–gel-induced reorganization of the first agar network.

3.5. Interfacial Toughness of Agar/pHEAA@MPS-CSNPs Gels. As known, agar and pHEAA networks possess abundant hydrophilic groups (-OH); thus, it is possible for agar/pHEAA@MPS-CSNPsgels to possess hydrogen-bondinginduced adhesion on solid surfaces. To prove this hypothesis, the surface adhesion ability of agar/pHEAA@MPS-CSNPs gels and agar/pHEAA gels on various nonporous substrates (glass, ceramics, titanium, and aluminum) was conducted by using the 90° peeling tests with a peeling rate of 50 mm/min. The stable peeling force curves in Figure 7A show that as a control agar/pHEAA DN gels can be strongly adhesive on glass, ceramics, titanium, and aluminum, generating high interfacial toughness (e.g., adhesion strength) of 3100 J/m² on glass, 1800 J/m² on ceramics, 1790 J/m² on titanium, and 1710 J/m² on aluminum (Figure 7E), while compared to agar/ pHEAA DN gels, three agar/pHEAA@MPS-CSNPs gels showed the reduced interfacial toughness after cross-linking with MPS-CSNPs. Fortunately, three agar/pHEAA@MPS-CSNPs gels remained a strong adhesion on various nonporous substrates (Figure 7B-D). For example, after introduction of

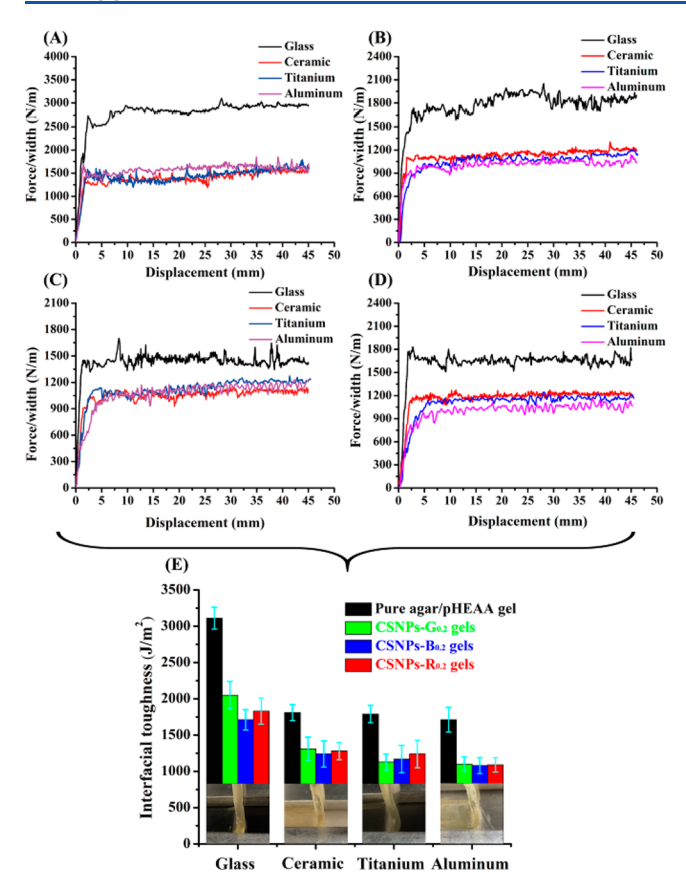


Figure 7. Curve of peeling force per width of (A) agar/pHEAA, (B) CSNPs- $G_{0.2}$, (C) CSNPs- $B_{0.2}$, and (D) CSNPs- $R_{0.2}$ gels on various nonporous solid substrates (titanium, ceramic, aluminum, and glass) under a fixed peeling rate of 50 mm/min. (E) Interfacial toughness of the above-mentioned hydrogels on different solid substrates.

MPS-CSNPs-G, the interfacial toughness of CSNPs- $G_{0.2}$ gels was 2050 J/m⁻² on glass, 1310 J/m⁻² on ceramic, 1130 J/m⁻²

on titanium, and 1102 J/m⁻² on aluminum. It is likely that the cross-linking of MPS-CSNP with polyHEAA network consumes some adhesive groups so as to loss their interfacial toughness to less extent. Additionally, MPS-CSNPs mainly contained hydrophobic groups, which further reduce the interfacial toughness of agar/pHEAA@MPS-CSNPs gels. Our previous works have demonstrated that hydrophobic PTFE surface exhibit very poor adhesion ability on different solid surfaces due to the decrease of hydrogen bonds between the gel and surface.³⁸

3.6. Upconversion Fluorescence Properties of Agar/ pHEAA@MPS-CSNPs Gels. The content effects of MPS-CSNPs on the fluorescence performance of three agar/ pHEAA@MPS-CSNPs gels were further studied. As shown in insets of Figures 8A-C, all three agar/pHEAA@MPS-CSNPs gels were transparent under daylight, but they can emit pure green, blue, and red UC fluorescence under 980 nm excitation, in sharp contrast to no fluorescence for agar/ pHEAA DN gels. Qualitatively, Figures 8A-C show the fluorescence spectra of three hydrogels with a continuous increase in the concentration of MPS-CSNPs from 0.1 to 1.0 wt %. In all three hydrogels, the fluorescence intensity increased as the concentration of MPS-CSNPs. The enhanced UC fluorescence is likely attributed to the large separation distance of MPS-CSNPs in the gels (more than hundreds of nanometers), which reduces the quenching in UC fluorescence. Under 980 nm excitation, CSNPs-G, CSNPs-B, and CSNPs-R gels emitted green (Figure 8A), blue (Figure 8B), and red (Figure 8C) UC fluorescence, respectively. Specifically, two major fluorescence peaks at 527 and 541 nm of CSNPs-G gels (Figure 8A) were exactly the same as those of MPS-CSNPs-G (Figure S2A). The same major fluorescence peaks were also observed between CSNPs-B gels and MPS-CSNPs-B at 450 and 475 nm and between CSNPs-R gels and MPS-CSNPs-R at 644 nm. This indicates that MPS-CSNPs is a sole source of fluorescence when cross-linking with a hydrogel network.

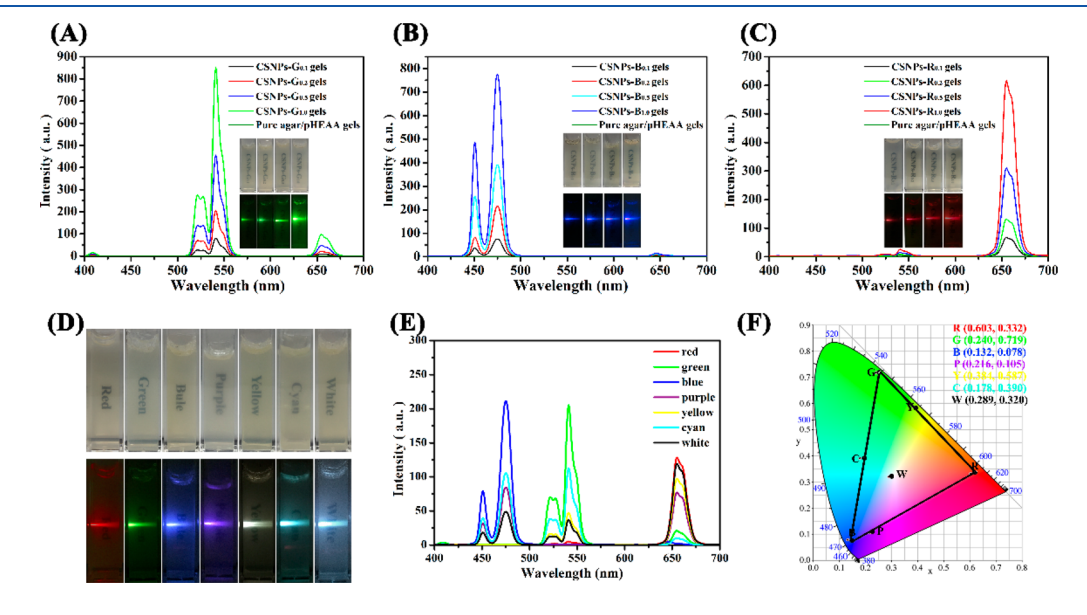


Figure 8. Concentration effect of MPS-CSNPs on the fluorescence properties of (A) CSNPs-G, (B) CSNPs-B, and (C) CSNPs-R gels. The insets show fluorescence images of three hydrogels under daylight (upper) and near-infrared light of 980 nm (bottom). (D) Optical photographs, (E) UC fluorescence spectra, and (F) corresponding CIE color coordinates of red, green, blue, purple, yellow, cyan, and white emitting agar/pHEAA@ MPS-CSNP gels. All hydrogels were prepared at a fixed concentration of CSNPs (1 wt %).

Upon obtaining agar/pHEAA@MPS-CSNP gels with pure green, blue, and red UC emission, we continued to fabricate full-color UC emission agar/pHEAA@MPS-CSNPs gels by copolymerizing and cross-linking different CSNPs chromophores with pHEAA network. Considering that the UC fluorescent intensity and their peak locations of the green, blue, and red emission are different under the same excitation conditions, it is critical for adjusting the content of CSNPs to achieve the hydrogel with desirable UC fluorescent color. As shown in Figure 8D and Table S1, agar/pHEAA@MPS-CSNP gels with secondary UC emission colors (cyan, magenta, yellow, and white) were obtained by copolymerizing different types and contents of MPS-CSNPs.

As a proof-of-concept example, we obtained cyan-emitting agar/pHEAA@MPS-CSNP gels by cross-linking both greenemitting MPS-CSNPs-G and blue-emitting MPS-CSNPs-B with pHEAA network at a molar ratio of MPS-CSNPs-G:MPS-CSNPs-B = 2:3. Because of the assembly of different independent green- and blue-emission MPS-CSNPs, different MPS-CSNPs of the resulting cross-linking gels were able to show other color simultaneously at different wavelengths and to emit mixed colors of cyan, as evidenced by the emission peaks of both Er3+ and Tm3+ in the photoluminescence spectra (Figure 8E). Following a similar strategy, purple, yellow, and white-emitting agar/pHEAA@MPS-CSNP gels were also prepared by adjusting the contents ratio of MPS-CSNPs-G, MPS-CSNPs-B, and MPS-CSNPs-R at 1:0:5, 0:1:2, and 1:1.5:7.5, respectively. Based on the UC luminescent spectra of agar/pHEAA@MPS-CSNP gels, the corresponding color coordinates were estimated and located into the Commission Internationale de l'Eclairage (CIE) chromaticity diagram. For example, the three primary UC emission color coordinates of red, green, and blue emitting agar/pHEAA@MPS-CSNP gels were (0.603, 0.332), (0.240, 719), and (0.132, 0.078), while the secondary emission colors of purple, yellow, and cyan were located at (0.216, 0.105), (0.384, 0.527), and (0.178, 0.390), respectively (Figure 8F). The white color coordinate of (0.289, 0.320) was very close to the ideal one with chromaticity coordinates of (0.333, 0.333). In principle, other hydrogels with any secondary fluorescent color can be obtained within a CIE triangle determined by three primary red, green, and blue color coordinates. In addition, we further challenged the longterm fluorescence stability of three agar/pHEAA@MPS-CSNP gels. As shown in Figure S7, the fluorescence intensity of the gels remained almost unchanged even upon exposure of the three agar/pHEAA@MPS-CSNP gels to ambient surroundings for 60 days, indicating the high fluorescence stability of CSNPs in the hydrogel network.

As a typical application example, we fabricated a novel self-healing agar/pHEAA@MPS-CSNPs hydrogel film with luminescent pattern (Figure 9A). Interestingly, the luminescent patterns were invisible by the naked eye. But, under 980 nm irradiation, they can be emitted multicolor patterns including red "H", green "U", and blue "T" patterns (Figure 9B). Because of the self-healing ability of agar/pHEAA gels, after cutting, agar/pHEAA gels film can self-heal together and still maintain their colorful fluorescence emission and intact information. Considering the advantages of superior upconversion fluorescence property, highly mechanical property, strong surface adhesion, and self-healing ability, an agar/pHEAA film with luminescent pattern demonstrates its promising for anticounterfeiting application.

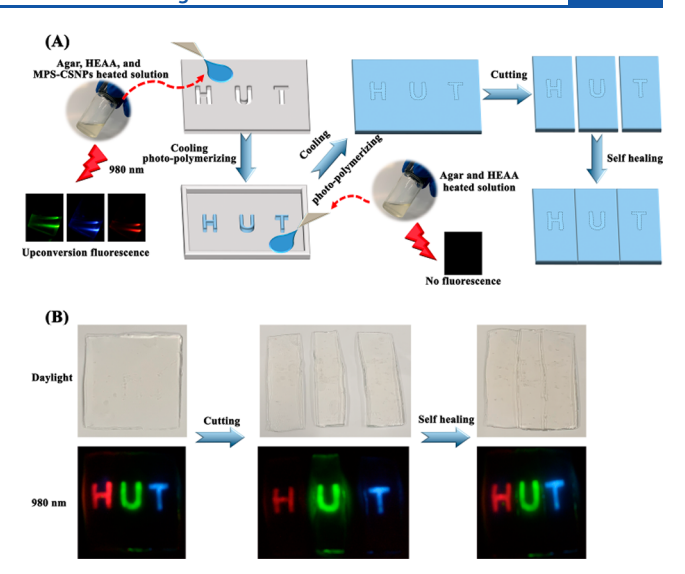


Figure 9. (A) Schematic presentation of the stepwise preparation of agar/pHEAA hydrogels with predesigned luminescent patterns. (B) Photographs of agar/pHEAA hydrogels with predesigned luminescent patterns before cutting and after healing; the photographs were visualized under 980 nm irradiation.

4. CONCLUSIONS

In summary, novel tough and fluorescent agar/pHEAA@MPS-CSNPs gels have been successfully developed in this work by incorporating the preformed NaREF₄:Ln³⁺@NaYF₄CSNPs fluorophores into the agar/HEAA hydrogel. The successful incorporation of MPS-NaREF₄:Ln³⁺@NaYF₄CSNPs (i.e., MPS-CSNPs) was achieved by covalent bonds between MPS-NaREF₄:Ln³⁺@NaYF₄CSNPs and the second pHEAA network, which simultaneously promote mechanical and fluorescence properties. First, the as-obtained agar/pHEAA@ MPS-CSNPs gels can achieve excellent high mechanical properties with a fracture stress of 2.4 MPa, a fracture strain of 5.6, a tearing energy of 11000 J/m², and a high toughness/ stiffness recovery of 47%/23% after 30 min resting at an elevated temperature of 95 °C. Because of the existence of reversible hydrogen bondings and other physical coordinate bonds between the networks and between networks and surfaces of solid surfaces, all three agar/pHEAA@MPS-CSNPs gels also can perform strong surface adhesion on different solid surfaces, as demonstrated by the high interfacial toughness of 1100-2000 J/m² on various solid surfaces (glass, aluminum, titanium, and ceramics). Third, the incorporation of green, blue, and red MPS-CSNPs into agar/pHEAA network endows the hydrogels to emit both primary (RGB) and any secondary (purple, yellow, cyan, and white) UC fluorescence colors under a 980 nm laser. Tunable full-color fluorescence of agar/ pHEAA@MPS-CSNPs hydrogels can be readily achieved by incorporating different types of MPS-CSNPs at proper ratios. Practically, we fabricated agar/pHEAA hydrogel film with fluorescence-responsive patterns. This work for the first time provides a novel design method to achieve a new hydrogel with highly tough, strong surface adhesion, full-color fluorescence for optical, imaging, anticounterfeiting, and sensing applications.

ASSOCIATED CONTENT

Supporting Information

The Supporting Information is available free of charge at https://pubs.acs.org/doi/10.1021/acsanm.0c00105.

Receipt of a series of agar/pHEAA@MPS-CSNPs with different contents of MPS-CSNPs; FTIR and fluorescence characterization of a series of MPS-CSNPs-based nanoparticles with different RGB emission colors; mechanical properties and hysteresis of agar/pHEAA@MPS-CSNPs hydrogels in response to the concentration of different network components; fluorescence stability of Agar/pHEAA@MPS-CSNPs hydrogels (PDF)

AUTHOR INFORMATION

Corresponding Authors

Jianxiong Xu — Hunan Key Laboratory of Biomedical Nanomaterials and Devices College of Life Sciences and Chemistry and National & Local Joint Engineering Research Center of Advanced Packaging Materials Developing Technology, Hunan University of Technology, Zhuzhou 412007, P. R. China; ⊚ orcid.org/0000-0001-5811-6880; Email: xujianxiong8411@163.com

Jie Zheng — Department of Chemical, Biomolecular, and Corrosion Engineering and Department of Polymer Engineering, The University of Akron, Akron, Ohio 44325, United States; orcid.org/0000-0003-1547-3612; Email: zhengj@uakron.edu

Authors

Shaowen Xie — Hunan Key Laboratory of Biomedical Nanomaterials and Devices College of Life Sciences and Chemistry and National & Local Joint Engineering Research Center of Advanced Packaging Materials Developing Technology, Hunan University of Technology, Zhuzhou 412007, P. R. China; Department of Chemical, Biomolecular, and Corrosion Engineering, The University of Akron, Akron, Ohio 44325, United States

Baiping Ren — Department of Chemical, Biomolecular, and Corrosion Engineering, The University of Akron, Akron, Ohio 44325, United States

Guo Gong — Hunan Key Laboratory of Biomedical Nanomaterials and Devices College of Life Sciences and Chemistry and National & Local Joint Engineering Research Center of Advanced Packaging Materials Developing Technology, Hunan University of Technology, Zhuzhou 412007, P. R. China

Dong Zhang — Department of Chemical, Biomolecular, and Corrosion Engineering, The University of Akron, Akron, Ohio 44325, United States

Yin Chen – Hunan Key Laboratory of Biomedical Nanomaterials and Devices College of Life Sciences and Chemistry, Hunan University of Technology, Zhuzhou 412007, P. R. China

Lijian Xu — Hunan Key Laboratory of Biomedical Nanomaterials and Devices College of Life Sciences and Chemistry and National & Local Joint Engineering Research Center of Advanced Packaging Materials Developing Technology, Hunan University of Technology, Zhuzhou 412007, P. R. China; ⊚ orcid.org/0000-0002-1195-6767

Changfan Zhang — National & Local Joint Engineering Research Center of Advanced Packaging Materials Developing Technology, Hunan University of Technology, Zhuzhou 412008, P. R. China

Complete contact information is available at: https://pubs.acs.org/10.1021/acsanm.0c00105

Author Contributions

S.X. and B.R. contributed equally to this work.

Notes

The authors declare no competing financial interest.

ACKNOWLEDGMENTS

J.Z. thanks the financial support from NSF (CMMI-1825122). J.X. thanks the financial support of the National Natural Scientific Foundation of China (51774129).

REFERENCES

- (1) Wen, S.; Zhou, J.; Zheng, K.; Bednarkiewicz, A.; Liu, X.; Jin, D. Advances in Highly Doped Upconversion Nanoparticles. *Nat. Commun.* **2018**, *9*, 2415.
- (2) Yuan, J.; Cen, Y.; Kong, X. J.; Wu, S.; Liu, C. L.; Yu, R. Q.; Chu, X. MnO₂-Nanosheet-Modified Upconversion Nanosystem for Sensitive Turn-On Fluorescence Detection of H₂O₂ and Glucose in Blood. *ACS Appl. Mater. Interfaces* **2015**, *7*, 10548–10555.
- (3) Li, H.; Wei, R.; Yan, G. H.; Sun, J.; Li, C.; Wang, H.; Shi, L.; Capobianco, J. A.; Sun, L. Smart Self-Assembled Nanosystem Based on Water-Soluble Pillararene and Rare-Earth-Doped Upconversion Nanoparticles for pH-Responsive Drug Delivery. ACS Appl. Mater. Interfaces 2018, 10, 4910–4920.
- (4) Li, N.; Lau, Y. S.; Xiao, Z.; Ding, L.; Zhu, F. NIR to Visible Light Upconversion Devices Comprising an NIR Charge Generation Layer and a Perovskite Emitter. *Adv. Opt. Mater.* **2018**, *6*, 1801084.
- (5) Kumar, A.; Reddy, K. L.; Kumar, S.; Kumar, A.; Sharma, V.; Krishnan, V. Rational Design and Development of Lanthanide-Doped NaYF₄@CdS-Au-RGO as Quaternary Plasmonic Photocatalysts for Harnessing Visible—Near-Infrared Broadband Spectrum. ACS Appl. Mater. Interfaces 2018, 10, 15565—15581.
- (6) Bhattacharya, S.; Phatake, R. S.; Nabha, B. S.; Zerby, N.; Zhu, J. J.; Shikler, R.; Lemcoff, N. G.; Jelinek, R. Fluorescent Self-Healing Carbon Dot/Polymer Gels. ACS Nano 2019, 13, 1433–1442.
- (7) Russell, G. M.; Inamori, D.; Masai, H.; Tamaki, T.; Terao, J. Luminescent and Mechanical Enhancement of Phosphorescent Hydrogel Through Cyclic Insulation of Platinum-acetylide Crosslinker. *Polym. Chem.* **2019**, *10*, 5280–5284.
- (8) Li, Y.; Young, D. J.; Loh, X. J. Fluorescent Gels: A Review of Synthesis, Properties, Applications and Challenges. *Mater. Chem. Front.* **2019**, *3*, 1489–1502.
- (9) Weng, D.; Zheng, X.; Chen, X.; Li, L.; Jin, L. Synthesis, Upconversion Luminescence and Magnetic Properties of New Lanthanide-Organic Frameworks with (43)2(46,66,83) Topology. *Eur. J. Inorg. Chem.* **2007**, 2007, 3410–3415.
- (10) Barrera, E. W.; Madueño, Q.; Novegil, F. J.; Speghini, A.; Bettinelli, M. Luminescence Upconversion of Er:Yb:KY(WO₄)₂ Green Phosphor with High Color Purity. *Opt. Mater.* **2018**, *84*, 354–359.
- (11) Wong, K. L.; Kwok, W. M.; Wong, W. T.; Phillips, D. L.; Cheah, K. W. Green and Red Three-Photon Upconversion from Polymeric Lanthanide(III) Complexes. *Angew. Chem., Int. Ed.* **2004**, 43, 4659–4662.
- (12) Xie, J.; Xie, X.; Mi, C.; Gao, Z.; Pan, Y.; Fan, Q.; Su, H.; Jin, D.; Huang, L.; Huang, W. Controlled Synthesis, Evolution Mechanisms, and Luminescent Properties of ScFx:Ln (x = 2.76, 3) Nanocrystals. *Chem. Mater.* **2017**, 29, 9758–9766.
- (13) Runowski, M.; Lis, S. Preparation and Photophysical Properties of Luminescent Nanoparticles Based on Lanthanide Doped Fluorides (LaF₃:Ce³⁺, Gd³⁺, Eu³⁺), Obtained in the Presence of Different Surfactants. *J. Alloys Compd.* **2014**, 597, 63–71.

- (14) Gao, W.; Dong, J.; Wang, Z.; Zhang, Z.; Zheng, H. Multicolor Upconversion Emission of Lanthanide-doped Single LiYF₄ and LiLuF₄ Microcrystal. *Mater. Res. Bull.* **2017**, *91*, 77–84.
- (15) Xie, S.; Tong, C.; Tan, H.; Li, N.; Gong, L.; Xu, J.; Xu, L.; Zhang, C. Hydrothermal Synthesis and Inkjet Printing of Hexagonal-phase NaYF₄: Ln³⁺ Upconversion Hollow Microtubes for Smart Anti-counterfeiting Encryption. *Mater. Chem. Front.* **2018**, *2*, 1997–2005.
- (16) Tan, H.; Gong, G.; Xie, S.; Song, Y.; Zhang, C.; Li, N.; Zhang, D.; Xu, L.; Xu, J.; Zheng, J. Upconversion Nanoparticles@Carbon Dots@Meso-SiO₂Sandwiched Core-shell Nanohybrids with Tunable Dual-mode Luminescence for 3D Anti-counterfeiting Barcodes. Langmuir **2019**, 35, 11503–11511.
- (17) Niu, N.; Zhang, Z.; Gao, X.; Chen, Z.; Li, S.; Li, J. Photodynamic Therapy in Hypoxia: Near-infrared-sensitive, Self-supported, Oxygen Generation Nano-platform Enabled by Upconverting Nanoparticles. *Chem. Eng. J.* 2018, 352, 818–827.
- (18) Dong, H.; Sun, L. D.; Yan, C. H. Energy Transfer in Lanthanide Upconversion Studies for Extended Optical Applications. *Chem. Soc. Rev.* **2015**, *44*, 1608–1634.
- (19) Gong, G.; Song, Y.; Tan, H.; Xie, S.; Zhang, C.; Xu, L.; Xu, J.; Zheng, J. Design of Core/Active-shell NaYF₄:Ln³⁺@NaYF₄:Yb³⁺ Nanophosphors with Enhanced Red-green-blue Upconversion Luminescence for Anti-counterfeiting Printing. *Composites, Part B* **2019**, *179*, 107504.
- (20) Wang, Z.; Gai, S.; Wang, C.; Yang, G.; Zhong, C.; Dai, Y.; He, F.; Yang, D.; Yang, P. Self-assembled Zinc Phthalocyanine Nanoparticles as Excellent Photothermal/Photodynamic Synergistic Agent for Antitumor Treatment. *Chem. Eng. J.* **2019**, *361*, 117–128.
- (21) Liu, Y.; Meng, X.; Bu, W. Upconversion-based Photodynamic Cancer Therapy. *Coord. Chem. Rev.* **2019**, *379*, 82–98.
- (22) Homann, C.; Krukewitt, L.; Frenzel, F.; Grauel, B.; Würth, C.; Resch-Genger, U.; Haase, M. NaYF₄:Yb,Er/NaYF₄ Core/Shell Nanocrystals with High Upconversion Luminescence Quantum Yield. *Angew. Chem., Int. Ed.* **2018**, *57*, 8765–8769.
- (23) Wang, W. N.; Huang, C. X.; Zhang, C. Y.; Zhao, M. L.; Zhang, J.; Chen, H. J.; Zha, Z. B.; Zhao, T.; Qian, H. S. Controlled Synthesis of Upconverting Nanoparticles/ZnxCd1-xS Yolk-shell Nanoparticles for Efficient Photocatalysis Driven by NIR Light. *Appl. Catal.*, B 2018, 224, 854–862.
- (24) Sun, Q.; He, F.; Sun, C.; Wang, X.; Li, C.; Xu, J.; Yang, D.; Bi, H.; Gai, S.; Yang, P. Honeycomb-satellite Structured pH/H₂O₂-responsive Degradable Nanoplatform for Efficient Photodynamic Therapy and Multimodal Imaging. *ACS Appl. Mater. Interfaces* **2018**, *10*, 33901–33912.
- (25) Xu, J.; Feng, Y.; Wu, Y.; Li, Y.; Ouyang, M.; Zhang, X.; Wang, Y.; Wang, Y.; Xu, L. Noninvasive Monitoring of Bone Regeneration Using NaYF₄: Yb³⁺, Er³⁺ Upconversion Hollow Microtubes Supporting PLGA-PEG-PLGA hydrogel. *React. Funct. Polym.* **2019**, 143, 104333.
- (26) Ye, C.; Ma, J.; Chen, S.; Ge, J.; Yang, W.; Zheng, Q.; Wang, X.; Liang, Z.; Zhou, Y. Eco-Friendly Solid-State Upconversion Hydrogel with Thermoresponsive Feature as the Temperature Indicator. *J. Phys. Chem. C* 2017, 121, 20158–20164.
- (27) Xiao, Q.; Li, Y.; Li, F.; Zhang, M.; Zhang, Z.; Lin, H. Rational Design of a Thermalresponsive-Polymer-Switchable FRET System for Enhancing the Temperature Sensitivity of Upconversion Nanophosphors. *Nanoscale* **2014**, *6*, 10179–10186.
- (28) Antoniadou, M.; Pilch-Wrobel, A.; Riziotis, C.; Bednarkiewicz, A.; Tanasă, E.; Krasia-Christoforou, T. Fluorescent Electrospun PMMA Microfiber Mats with Embedded NaYF₄: Yb/Er Upconverting Nanoparticles. *Methods Appl. Fluoresc.* **2019**, *7*, 034002.
- (29) Mader, H. S.; Wolfbeis, O. S. Optical Ammonia Sensor Based on Upconverting Luminescent Nanoparticles. *Anal. Chem.* **2010**, *82*, 5002–5004.
- (30) Wu, J.; Qin, Y. Polymeric Optodes Based on Upconverting Nanorods for Fluorescence Measurements of Pb2+ in Complex Samples. Sens. Actuators, B 2014, 192, 51–55.
- (31) Meier, R. J.; Simbürger, J. M. B.; Soukka, T.; Schaferling, M. Background-Free Referenced Luminescence Sensing and Imaging of

- pH Using Upconverting Phosphors and Color Camera Read-out. *Anal. Chem.* **2014**, *86*, 5535–5540.
- (32) Shin, J.; Kyhm, J. H.; Hong, A. R.; Song, J. D.; Lee, K.; Ko, H.; Jang, H. S. Multicolor Tunable Upconversion Luminescence from Sensitized Seed-mediated Grown LiGdF₄:Yb,Tm-based Core/Tripleshell Nanophosphors for Transparent Displays. *Chem. Mater.* **2018**, 30, 8457–8464.
- (33) Dong, Y.; Lin, M.; Jin, G.; Il Park, Y.; Qiu, M.; Zhao, Y.; Yang, H.; Li, A.; Jian Lu, T. Fabrication of Fluorescent Composite Hydrogel Using in Situ Synthesis of Upconversion Nanoparticles. *Nanotechnology* **2017**, *28*, 175702.
- (34) Jalani, G.; Naccache, R.; Rosenzweig, D. H.; Haglund, L.; Vetrone, F.; Cerruti, M. Photocleavable Hydrogel-coated Upconverting Nanoparticles: A Multifunctional Theranostic Platform for NIR Imaging and On-demand Macromolecular Delivery. *J. Am. Chem. Soc.* **2016**, *138*, 1078–1083.
- (35) Yan, B.; Boyer, J. C.; Habault, D.; Branda, N. R.; Zhao, Y. Near Infrared Light Triggered Release of Biomacromolecules from Hydrogels Loaded with Upconversion Nanoparticles. *J. Am. Chem. Soc.* **2012**, *134*, 16558–16561.
- (36) Zhou, L.; Chen, E.; Jin, W.; Wang, Y.; Zhou, J.; Wei, S. Monomer Zinc Phthalocyanine/Upconversion Nanoparticle Coated with Hyaluronic Acid Crosslinked Gel as NIR Light-activated Rug for in Vitro Photodynamic Therapy. *Dalton Trans.* **2016**, *45*, 15170–15179.
- (37) Zhang, W.; Miao, W.; Yue, Z.; Liu, S.; Li, L.; Zhang, Z.; Wang, H. Glow Discharge Electrolysis Plasma Initiated Synthesis of Upconversion Luminescent and Temperature Sensitive Multifunctional Hydrogel. *Soft Mater.* **2018**, *16*, 192–200.
- (38) Chen, Q.; Zhu, L.; Zhao, C.; Wang, Q.; Zheng, J. A Robust, One-pot Synthesis of Highly Mechanical and Recoverable Double Network Hydrogels Using Thermoreversible Sol-gel Polysaccharide. *Adv. Mater.* **2013**, 25, 4171–4176.
- (39) Kurokawa, T.; Furukawa, H.; Wang, W.; Tanaka, Y.; Gong, J. P. Formation of a Strong Hydrogel–porous Solid Interface Via the Double-network Principle. *Acta Biomater.* **2010**, *6*, 1353–1359.
- (40) Yuk, H.; Zhang, T.; Lin, S.; Parada, G. A.; Zhao, X. Tough Bonding of Hydrogels to Diverse Non-porous Surfaces. *Nat. Mater.* **2016**, *15*, 190.
- (41) Zhang, Y.; Ren, B.; Xie, S.; Cai, Y.; Wang, T.; Feng, Z.; Tang, J.; Chen, Q.; Xu, J.; Xu, L.; Zheng, J. Multiple Physical Cross-linker Strategy to Achieve Mechanically Tough and Reversible Properties of Double-network Hydrogels in Bulk and on Surfaces. *ACS Appl. Polym. Mater.* **2019**, *1*, 701–713.
- (42) Xie, S.; Gong, G.; Song, Y.; Tan, H.; Zhang, C.; Li, N.; Zhang, Y.; Xu, L.; Xu, J.; Zheng, J. Design of Novel Lanthanide-doped Coreshell Nanocrystals with Dual Up-conversion and Down-conversion Luminescence for Anti-counterfeiting Printing. *Dalton Trans.* **2019**, 48, 6971–6983.
- (43) Na, H.; Woo, K.; Lim, K.; Jang, H. S. Rational Morphology Control of β -NaYF₄:Yb,Er/Tm Upconversion Nanophosphors Using a Ligand, an Additive, and Lanthanide Doping. *Nanoscale* **2013**, *S*, 4242–4251.
- (44) Yang, D.; Cao, C.; Feng, W.; Huang, C.; Li, F. Synthesis of NaYF₄:Nd@NaLuF₄@SiO₂@PS Colloids for Fluorescence Imaging in the Second Biological Window. *J. Rare Earths* **2018**, *36*, 113–118.
- (45) Chen, H.; Liu, Y.; Ren, B.; Zhang, Y.; Ma, J.; Xu, L.; Chen, Q.; Zheng, J. Super Bulk and Interfacial Toughness of Physically Crosslinked Double-network Hydrogels. *Adv. Funct. Mater.* **2017**, 27, 1703086.
- (46) You, W.; Tu, D.; Zheng, W.; Shang, X.; Song, X.; Zhou, S.; Liu, Y.; Li, R.; Chen, X. Large-scale Synthesis of Uniform Lanthanide-doped NaREF₄ Upconversion/Downshifting Nanoprobes for Bioapplications. *Nanoscale* **2018**, *10*, 11477–11484.
- (47) Mai, H. X.; Zhang, Y. W.; Si, R.; Yan, Z. G.; Sun, L. d.; You, L. P.; Yan, C. H. High-Quality Sodium Rare-Earth Fluoride Nanocrystals: Controlled Synthesis and Optical Properties. *J. Am. Chem. Soc.* **2006**, 128, 6426–6436.

- (48) Li, X.; Wang, H.; Wang, T.; Wang, L.; Liu, X.; Zhu, X. Preparation of NaYF₄:Yb, Er Nanoparticles Coated with Hydrophilic Polystyrene. *Mater. Lett.* **2019**, 247, 159–162.
- (49) Javaheri, F.; Hassanajili, S. Synthesis of Fe₃O₄@SiO₂@MPS@P₄VP Nanoparticles for Nitrate Removal from Aqueous Solutions. *J. Appl. Polym. Sci.* **2016**, 133.
- (50) Du, G.; Song, Y.; Li, N.; Lijian, X.; Tong, C.; Feng, Y.; Chen, T.; Xu, J. Cage-like Hierarchically Mesoporous Hollow Silica Microspheres Templated by Mesomorphous Polyelectrolyte-Surfactant Complexes for Noble Metal Nanoparticles Immobilization. *Colloids Surf., A* **2019**, *575*, 129–139.
- (51) Wang, F.; Wang, J.; Liu, X. Direct Evidence of a Surface Quenching Effect on Size-Dependent Luminescence of Upconversion Nanoparticles. *Angew. Chem., Int. Ed.* **2010**, *49*, 7456–7460. (52) Shang, Y.; Hao, S.; Lv, W.; Chen, T.; Tian, L.; Lei, Z.; Yang, C.
- (52) Shang, Y.; Hao, S.; Lv, W.; Chen, T.; Tian, L.; Lei, Z.; Yang, C. Confining Excitation Energy of Er³⁺-sensitized Upconversion Nanoparticles Through Introducing Various Energy Trapping Centers. *J. Mater. Chem. C* **2018**, *6*, 3869–3875.